

Structural and optical characterization of single nanoparticles and single molecule SERS

Samuel L. Kleinman^a, Julia M. Bingham^a, Anne-Isabelle Henry^a, Kristin L. Wustholz^a,
Richard P. Van Duyne^{*a}

^aNorthwestern University, Department of Chemistry, 2145 Sheridan Rd., Evanston, IL
60208

ABSTRACT

Although plasmonic nanoparticles are widely utilized in spectroscopy and sensing applications, a quantitative structure-function relationship is lacking. In this proceeding, we discuss measurements of single noble metal nanoparticles using localized surface plasmon resonance (LSPR) spectroscopy, surface-enhanced Raman spectroscopy (SERS), and transmission electron microscopy (TEM) to elucidate structure-function relationships. A recently developed LSPR imaging spectroscopy instrument with an extremely fast camera enables measurement of diffusion constants for individual silver nanoprisms dispersed in water—paving the way for plasmonic particles as dynamic labels in biological systems. Correlated studies involving two or all three of these techniques relate optical properties of the *same* nanoparticle to its structure. Lastly, single-molecule surface-enhanced Raman spectroscopy of Rhodamine 6G is explored on lithographically fabricated plasmonic structures.

Keywords: Localized surface plasmon resonance, surface-enhanced Raman spectroscopy, Rhodamine, SERS nanotags, nanoprisms, single-nanoparticle spectroscopy, wide-field imaging, transmission electron microscopy

1. INTRODUCTION

Noble metal nanoparticles have unique optical properties that have been utilized since the time of the Roman Empire. They are present in brilliantly colored works of art such as the Lycurgus cup and stained glass windows as well as nanoscale optical sensors.^{1,2} Since the 19th century scientists have attempted to describe the fundamental physics underlying the optical properties of these particles.³ In modern times, this particular light-matter interaction is known as the localized surface plasmon resonance (LSPR). The LSPR is a result of oscillation of conduction electrons in a metal nanoparticle excited by incident electromagnetic radiation. The LSPR peak frequency and lineshape are sensitive to changes in particle morphology and local refractive index.² This moving charge is an oscillating dipole which creates a near-field enhancement of the intensity of incident radiation, giving rise to surface-enhanced spectroscopies. Transmission electron microscopy has allowed researchers to characterize nanoparticles on similar length scales, adding fundamental understanding to the effects of size, shape, composition, and surrounding dielectric medium on the LSPR extinction spectrum of a particular particle, aggregate, or array of particles.⁴ Plasmonics has been implemented in detection and quantification via surface-enhanced and LSPR spectroscopies. *In vivo* glucose sensing, disease biomarker and chemical warfare agent detection are a few prominent examples.⁵

Ensemble-averaged measurements on plasmonic particles reveal bulk LSPR response to changes in environment. Surface-enhanced Raman spectroscopy (SERS) on enhancing nanostructures provides detection for analytes with concentration down to the picomole regime.⁵ In some cases, monitoring ensemble response is beneficial; such as employing a low resolution, maintenance, or sensitivity detection scheme. Single nanoparticle or single molecule spectroscopy provides insight into the ensemble response which can then be reconstructed from each of its constituent members.⁶ Analysis and optimization of each individual sensing event can improve the overall detection modality for applied studies. These spectroscopies probe the physical and electromagnetic environment of a particle or molecule revealing localized and specific

information. In this proceeding we employ both single molecule and single nanoparticle spectroscopy and investigate phenomena such as refractive index sensitivity, electromagnetic field enhancement, and nanostructure morphology as it relates to LSPR extinction. We apply a new high-speed wide-field LSPR imaging instrument to measure diffusion constants for single Ag nanoprisms in water. The instrument was also used to screen the refractive index response of many single nanoparticles in parallel, revealing heterogeneity in plasmonic response present in the products from a single reaction mixture.

Single molecule and single nanoparticle optical experiments can address many issues; however, some questions remain unanswered. Such as, what shape particle is the most responsive to refractive index changes? What other structural parameters affect the position and response of an LSPR-based sensor? Which nanostructures give the greatest SERS enhancement? Answering these questions will provide a set of guidelines for targeted synthesis of the most effective and useful plasmonic particles. We are now at a unique intersection of optical and electron microscopy which can begin to probe the effect of minute variations in nanoparticle structure on the plasmon resonance. Here, we discuss two correlated optical spectroscopy-transmission electron microscopy (TEM) experiments which provide insight unobtainable from a single measurement. Along with modulations in an individual particle or small aggregate LSPR spectrum, different shapes and cluster geometries have marked effects on SERS enhancing efficiency. Both fundamental and applied studies benefit from the optical and morphological characterization of noble metal nanoparticles, especially when used cooperatively.

The inherent abilities of Raman spectroscopy for detection, identification, and quantification make this technique an extremely useful analytical tool.^{7, 8} Normal Raman scattering is an infrequent event which can be difficult to observe. Surface-enhanced Raman spectroscopy (SERS) is normal Raman spectroscopy conducted on or very near plasmonic nanostructures that can enhance Raman signal by up to eight orders of magnitude. SERS has been used for molecular identification of trace analytes.⁹ The enhancement factor (EF) is a metric of SERS activity, most simply stated as the ratio of signal with SERS substrate to signal without SERS substrate, normalized by number of molecules. The enhancing efficiency of a SERS substrate varies within and between samples, materials, and preparation methods. The most effective sensing platform would ideally have strong and consistent SERS activity across the sensor surface. To create scalable plasmonic surfaces, many types of templating and lithography have been utilized.^{10, 11} We focus here on nanosphere lithography (NSL), a low-cost and high-throughput technique which can produce SERS substrates inches in size.¹²

The ultimate test for a SERS substrate is the capability to adequately enhance signal such that a single molecule can be observed. Two literature reports in 1997 claimed to observe SERS signal from a single molecule (SMSERS); however, there was no generally accepted proof of SMSERS.^{13, 14} Recently, methods for a rigorous proof of SMSERS have been utilized and one of these methods will be employed in this manuscript.^{15, 16} The 'bi-analyte' SMSERS scheme involves mixing two Raman-active probe molecules with distinct vibrational spectra in equimolar dilute concentrations and depositing them on a SERS substrate.¹⁵ Upon measuring the SERS signal, if a majority of the time, a signature from only one *or* the other is measured, it can be statistically proven that the signal is indeed coming from just *one* molecule. In 2007 this method was augmented by introducing isotopically-edited Raman probe molecules. R6G was synthesized with four deuterium nuclei on the lone ring. Subsequently, R6G- d_0 and R6G- d_4 were used as bi-analyte SERS probes, resulting in observation of signal from only one isotopologue even though both are present on the substrate.¹⁶ SMSERS measurements are commonly conducted on Ag colloids that are randomly aggregated by salt addition, thus making them highly irreproducible. Lithographically created SERS substrates offer advantages, such as scalability, tunable effective spectral range, and better substrate reproducibility. It has not yet been conclusively demonstrated that these substrates can yield SERS signal from a single molecule,¹⁷ hence, we chose to explore lithographically created substrates using the R6G isotopologue pair to establish single-molecule sensitivity.

We perform measurements of single nanoparticles to determine the refractive index sensitivity, and separately use LSPR spectra to track the motion of single nanoprisms and determine diffusion constants for the prisms in water. We then use a correlated LSPR-TEM technique to elucidate structure-function relationships within

single Ag nanoprisms. A correlated LSPR-SERS-TEM scheme is applied to analyze single small aggregates of spherical Au particles for nanostructure, LSPR spectra and SERS efficiency. Also, SMSERS is explored on lithographically fabricated periodic particle arrays (PPA).

2. METHODOLOGY

2.1 Materials

Deionized water was used for all experiments (Millipore Milli-Q, 18.2 M Ω /cm). Silver nanoprisms were synthesized following a previously published literature procedure.¹⁸ In short, 0.3 mM sodium citrate (Sigma-Aldrich) was added to 0.1 mM AgNO₃ (aq, Sigma-Aldrich) and stirred on ice. Cold 50 mM NaBH₄ (1 mL, Sigma-Aldrich) was then added. A solution of 5 mM bis(*p*-sulfonatophenyl)-phenylphosphine dehydrate dipotassium (BSPP, 1 mL, Strem Chemicals) was added dropwise to stabilize the growing particles in solution. Strong stirring on ice was continued for 1 h, followed by 3-4 h of mild stirring over ice, resulting in a yellow solution which was subsequently irradiated for 4-5 h with 550 nm light. The solution turned green during the irradiation process as a result of nanoprism growth. The solution was then centrifuged and resuspended twice in water. Nanoprisms were immobilized for refractive index sensitivity analysis in a polydimethylsiloxane (PDMS, Dow Corning) flow cell using aminopropyltrimethoxysilane (APTMS, Sigma-Aldrich). A 1% solution of APTMS in methanol was added into the PDMS flow cell and allowed to sit for at least 1 h. The cell was then rinsed thoroughly with methanol and water and dried with compressed air. Functionalizing the glass with APTMS made the glass positively charged such that negatively charged nanoparticles would be immobilized. Approximately 1 mL of diluted nanoprism solution (diluted 1:10 in water) was added to the flow cell and the nanoparticles were left to bind for at least 1 h or as long as overnight, followed by rinsing in water. Samples of nanoprisms in solution for two-dimensional diffusion analysis employed a PDMS microfluidic channel as a flow cell for nanoparticles diluted 1:10 in water.

SERS nanotags are dimers, trimers, and larger aggregates of 100 nm Au spheres coated in a probe molecule, 2-(4-Pyridyl)-2-cyano-1-(4-ethynylphenyl)ethylene, (PCEPE), and encased in a 50 nm thick SiO₂ shell. The nanotags were used as received from Oxonica Inc. The nanotag solution (10 μ L) was deposited on a 200 mesh TEM grid (Ted Pella) by drop-coating for correlated SERS-LSPR-TEM studies.

Periodic particle array (PPA) substrates for SMSERS measurements were created by NSL.¹² Briefly, 2 μ L of a 4% w/v solution of 290 nm diameter carboxyl-terminated polystyrene spheres (Duke Scientific) were drop-cast on piranha-cleaned and base-treated 18 mm #1 glass coverslips (Fisher Scientific), spread by gravitational flow, and allowed to dry into two-dimensional colloidal crystal masks. Silver (50 nm, Kurt J. Lesker Co., 99.999%) was subsequently deposited through these masks at a rate of 2 \AA /s (Kurt J. Lesker Co., AXXIS). Upon removal of the spheres, an array of triangular nanoparticles was left on the glass surface. Rhodamine 6G (R6G-*d*₀, Sigma-Aldrich) and deuterated rhodamine 6G (R6G-*d*₄, custom synthesis by Scheidt group at Northwestern University) were dissolved in water and mixed in equimolar concentrations (total 10⁻¹⁰ M dye) for SMSERS measurements. Dye mixture (20 μ L of 10⁻¹⁰ M) was spin-coated on PPA surfaces to provide coverage of <1 molecule per square micron. Ag island films (AgIFs) for reference R6G measurements were created by depositing 6 nm of Ag onto piranha-cleaned and base-treated coverslips, incubated in a 10⁻⁴ M R6G ethanolic solution overnight, then thoroughly rinsed with ethanol prior to spectroscopic measurements.

2.2 Wide-field LSPR spectroscopy

This relatively new technique has been detailed elsewhere.^{19, 20} Briefly, the wide-field LSPR spectroscopy experiments were performed on an inverted microscope (Nikon Eclipse Ti-U) with a 100x oil-immersion objective (Nikon, Plan Fluor, 100X, NA = 0.5-1.3) set to NA = 0.5. A quartz-tungsten halogen lamp and a dark-field condenser (Nikon, NA = 0.80-0.95) provided white light illumination. This geometry allows us to collect only the resonant Rayleigh scattered light from the nanoparticles. The scattered light from multiple nanoparticles was sent through a liquid crystal tunable filter (LCTF, CRi VariSpec), which has a continuously tunable transmission from 400 nm to 720 nm with a spectral bandwidth of 7 nm, to a LN₂-cooled CCD detector (Princeton Instruments Spec-10 400B). For refractive index sensitivity studies, the LCTF was scanned from

400 nm to 720 nm in 2 nm increments, collecting a series of wide-field intensity images, where each frame has associated wavelength information. Correlated widefield LSPR-TEM studies were accomplished by drop coating Ag nanoprisms onto a TEM grid (300 mesh, Ted Pella) which was placed on a clean glass #1 coverslip. Nanoparticle locations were noted in the optical microscope using TEM grid squares, located in the TEM, and imaged. The scattering intensity of each nanoparticle was integrated as a function of wavelength to construct single nanoparticle spectra. An EMCCD was used for diffusional dynamics studies, allowing shorter integration times. The LCTF was scanned from 400 nm to 720 nm in 1 nm increments at a fixed time interval (integration time 0.1 s, gain of 500) and a series of images were collected where each frame has associated wavelength and time information.

2.3 Surface-enhanced Raman & LSPR spectroscopy of SERS nanotags

SERS nanotag measurements were performed on an inverted microscope (Nikon TE300) fit with an oil immersion objective (Nikon, Plan Fluor, 100x, NA = 0.5-1.3), with NA set to 0.5. Collected signal was analyzed using a 1/3 m spectrograph with a 1200 grooves/mm grating and LN₂-cooled CCD (Acton 300i, SPEC-10 400B). For SERS measurements, the sample was placed on a microscope coverslip and excited with a HeNe laser (Research Electro-Optics, 17 mW) operating at 632.8 nm. The laser light was filtered using a bandpass filter (Semrock, NF03-633E-25), and individual nanotags were illuminated in an epi configuration. Backscattering was collected by the same objective used for excitation, filtered for Rayleigh scattered laser light using a long-pass filter (Semrock, LL01-633-25) and analyzed. Dark-field scattering LSPR measurements of individual SERS nanotags used a 150 grooves/mm grating for larger spectral range. Illumination for LSPR measurements was created by a quartz-tungsten halogen lamp directed through a dry dark-field condenser (Nikon, NA = 0.70-0.95). Using this geometry, only Rayleigh scattered light was detected.

2.4 Single-molecule and ensemble-averaged Surface-enhanced Raman spectroscopy of rhodamine 6G

The same microscope and detection system used in section 2.3 was used for rhodamine 6G studies. All samples were placed in a custom-built flow cell and immersed in a dry N₂ atmosphere. For ensemble-averaged measurements on AgIFs, epiillumination with 532 nm laser light (Spectra-Physics, Millennia X) was used for excitation, signal was collected in a backscattering geometry and filtered for residual laser light by a long-pass filter (Semrock, LP03-532RS-25). Laser light was focused (200 μW, 22 μm² waist) yielding a power density (P_{ex}) of ~ 900 W/cm². For SMSERS measurements on PPA samples, laser light was directed in a grazing incidence configuration with a 60° angle between the incident beam and the surface normal and focused (125 mW, ~ 50000 μm² ellipsoidal waist), yielding P_{ex} ~ 250 W/cm². Scattered light was collected, filtered and analyzed using equipment described above.

2.5 Transmission electron microscopy

A JEOL JEM-2100F Fast TEM operating at 200kV was used for TEM measurements of SERS nanotags. A Hitachi HD2300 STEM operating at 200 kV was used for measurements of Ag nanoprisms.

3. RESULTS AND DISCUSSION

3.1 Multiplexed LSPR refractive index sensitivity

Different shaped nanoparticles may have varying detection sensitivity when integrated into an optical sensor. The refractive index (RI) sensitivity of single nanoparticles had been examined previously using Ag colloids, Ag triangular nanoprisms, and Ag nanocubes.²¹⁻²³ However, relatively few nanoparticles were characterized due to the tedious experimental conditions associated with the spectrometer grating/slit method. Using the LCTF wide-field method described here, the RI sensitivities of 29 single Ag nanoprisms were determined simultaneously. Figure 1 displays a plot of the change in LSPR maximum wavelength ($\Delta\lambda_{\max}$) vs. RI for 7 distinct nanoprisms in 4 different media, representing the range of RI sensitivities present in the sample. The RI sensitivity ranged from 73 nanometers per refractive index unit (nm/RIU) to 260 nm/RIU. Polydispersity in the nanoprism reaction mixture results in an array of nanoparticle shapes. Many of the nanoparticles are

triangular nanoprisms; however, TEM studies have shown that trapezoids, hexagons, rods, and other shapes are present in the sample. It is possible to infer shape information from the RI sensitivity, based on previous correlated TEM-LSPR studies.²³ For example, the particle with the greatest RI response is likely a rod-shaped particle as particles with this morphology are commonly more sensitive to the local environment. However, without correlating each nanoparticle structure to its spectrum, the shape can not be confirmed with certainty by the spectrum or RI sensitivity value alone. The variety of RI sensitivity and products of the synthesis highlights the need for correlated structure-plasmonic activity measurements to best assess the most useful particles. Future experiments will focus on RI studies on a TEM grid so sensitivity can be correlated to structure with absolute certainty.

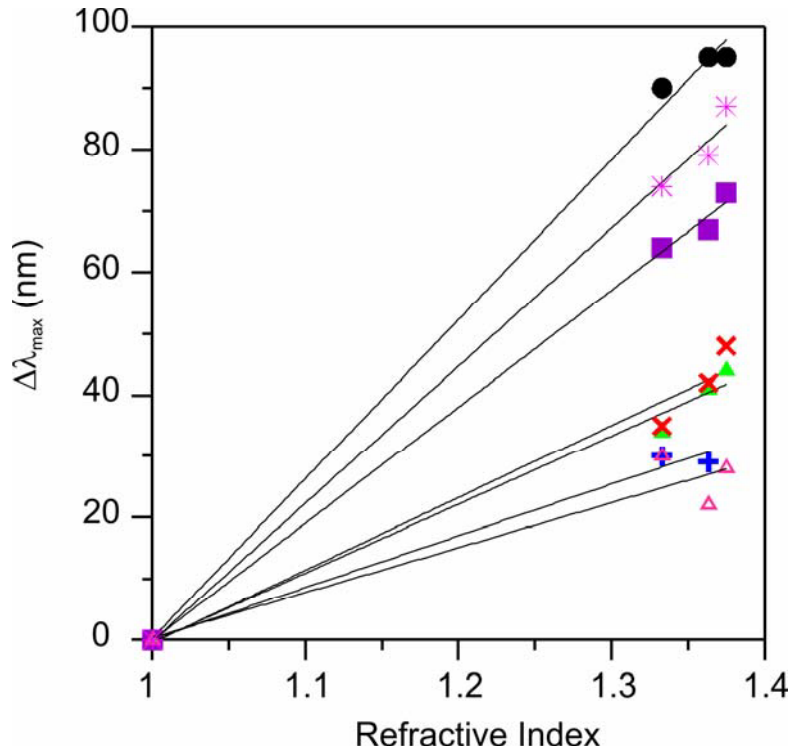


Figure 1. Solvent study on single triangular nanoprisms demonstrating the RI sensitivity, m , of 7 representative single nanoparticles. $m = 260$ (●), 225 (•), 190 (■), 118 (×), 112 (▲), 84 (+), and 73 (△) nm/RIU.

3.2 Diffusional dynamics studied by wide-field LSPR spectroscopy

The scattering spectrum of an individual nanoparticle is a direct probe into the local environment surrounding the particle.⁴ Coupling this measurement with nanoparticle diffusional dynamics can provide even more information about the viscosity of a local environment. Tracking nanoparticles in cells and through cellular processes could revolutionize the use of noble metal nanoparticles in molecular biology. Previously, single nanoparticle spectra and single particle trajectories were obtained simultaneously and in real time, but due to camera speed limitations, a highly viscous medium was required.¹⁹ Accordingly, our group has improved the wide-field LSPR analysis technique with an EMCCD, to decrease acquisition time to biologically relevant timeframes. Using the faster detector, longer integration times were not required and water was used. Single particle trajectories and mean square displacement for two particles are illustrated in Figure 2. The two particles had scattering spectra with $\lambda_{\text{max}} \sim 570$ nm and 621 nm for particle 1 and 2, respectively (not shown). It was determined that particle 1 had a diffusion coefficient of 9.0×10^{-8} cm²/s (corresponding to 24 nm radius) and particle 2 had a diffusion coefficient of 6.3×10^{-8} cm²/s (corresponding to 34 nm radius). These calculated

particle sizes are close to the actual size of Ag nanoprisms synthesized in a similar manner.¹⁸ The past two sections have demonstrated applications of plasmonic particles and it was possible to estimate the shape or size of the particles. However, in the next sections we will elucidate these relationships using correlated structural-optical experiments.

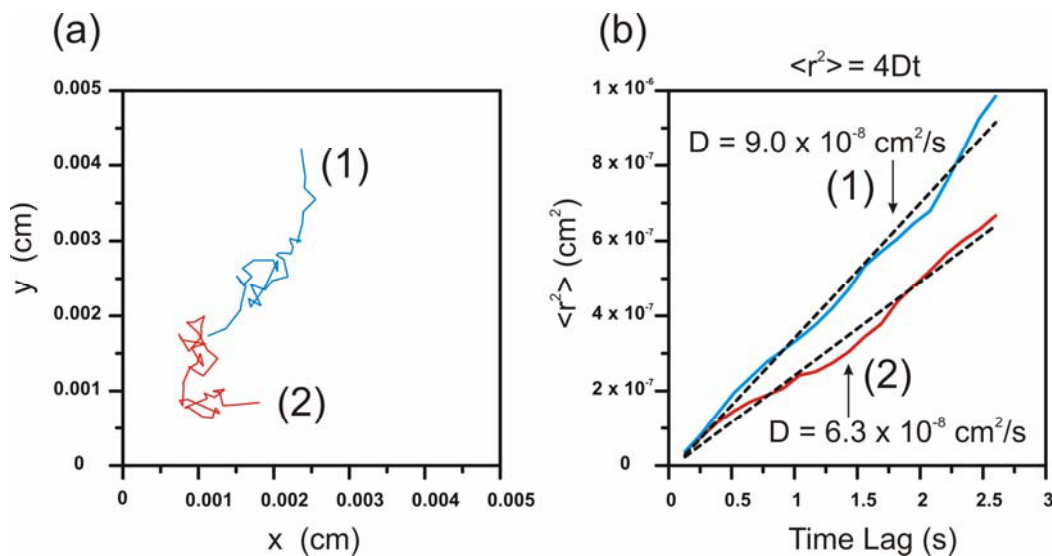


Figure 2. Diffusion studies on two individual Ag nanoprisms in water: (a) single particle trajectories for two single nanoparticles in water (1, blue; 2, red); (b) mean square displacement, $\langle r^2 \rangle$, plotted as a function of the time lag, t , for particles 1 and 2 and fit with a linear regression.

3.3 Correlated wide-field LSPR spectroscopy – transmission electron microscopy

Figure 3a shows LSPR spectra from two distinct Ag nanoprisms resulting from the same synthesis. They both have the same LSPR peak wavelength (645 nm), consistent with previous single nanoprism measurements. Although they have similar composition, shape, and LSPR peak wavelength, the linewidth of each particles' plasmon resonance is slightly different. In a single particle experiment without correlated structural characterization, it may be assumed that these two particles have similar size. Upon inspecting Figure 3b and c it is evident that the lower prism has a perpendicular bisector at least twice as long as the upper prism. The two-dimensional area of the lower prism is at least four times that of the upper prism. This observation highlights the strength of correlated spectroscopy-structure studies for elucidating relationships which are otherwise unobservable. It should be noted that the difference in contrast in TEM images is an artifact and has no physical meaning. Further inspection shows another structural difference between the particles—the roundedness or lack thereof for the triangular corners. Studies are underway to determine how this parameter affects the LSPR peak wavelength and linewidth. Correlated widefield LSPR-TEM studies allow us to relate LSPR spectra to commonly explored (size) and previously underexplored structural parameters (corner rounding). This experimental synergy will provide guidance for targeted synthesis of the most sensitive particles for integration into and optimization of optical biosensing platforms.

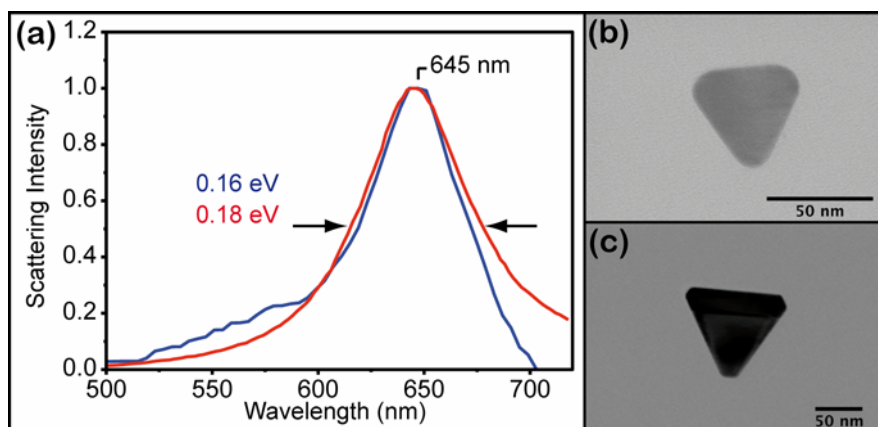


Figure 3. Correlated single particle data: (a) Two scattering spectra exhibiting plasmon resonance at the same wavelength (645 nm) and having similar linewidth; Corresponding TEM images of nanoparticles: (b) red spectrum; (c) blue spectrum.

3.4 Surface-enhanced Raman & LSPR spectroscopy of SERS nanotags

SERS nanotags are well-defined Au nanoparticle aggregates that are encased in a protective SiO₂ shell. We analyzed the EF distribution for 30 individual nanotags dispersed on a TEM grid. Figure 4a shows a histogram of the observed EFs, with individual values ranging from 6.6×10^6 to 4.8×10^8 . The EF was determined by comparison with liquid-phase normal Raman of the PCEPE probe molecule, structure in figure. Despite possessing various geometries and LSPR spectra, the EFs are within two orders of magnitude. To further investigate what structural parameters govern SERS efficiency, a correlated LSPR-TEM-SERS experiment was conducted on individual SERS nanotags. Figure 4b and c show TEM images of two different SERS nanotags with corresponding LSPR spectra. The gold cores that compose the nanotags are fairly monodisperse, suggesting that other structural motifs determine optical properties. The LSPR spectra are broad and contain multiple peaks, consistent with the aggregated morphology of the nanotags. Preliminary experimental and computational modeling suggest that interparticle spacing is the dominant factor in determining SERS activity as well as the LSPR spectrum.²⁴

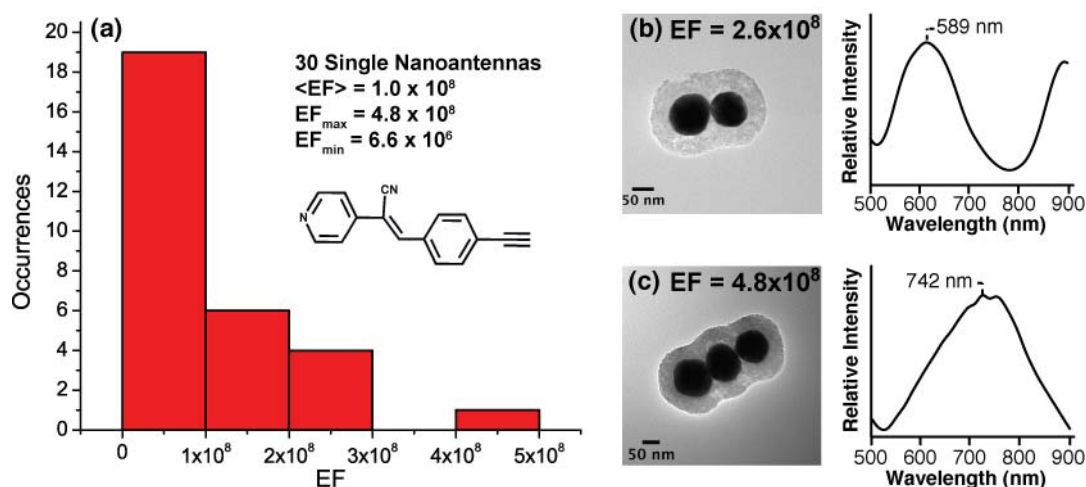


Figure 4. Analysis of SERS nanotags: (a) Histogram of enhancement factors for 30 nanotags, with PCEPE structure; TEM images of: (b) dimer and (c) trimer with corresponding EFs and LSPR spectra.

3.5 Single-molecule and ensemble-averaged surface-enhanced Raman spectroscopy of rhodamine 6G

The surface-enhanced resonance Raman spectra of R6G- d_0 and R6G- d_4 have been previously published and a spectrum of R6G- d_0 on a AgIF is presented in Figure 5a. This spectrum shows prominent peaks at 1659, 1584, 1516, 1365, 1327, 1193, 1130, 781, and 622 relative cm^{-1} , in agreement with literature precedent.¹⁶ Equimolar amounts of an extremely dilute solution (10^{-10} M) of the R6G isotopologue pair are deposited on the PPA via spin coating, promoting sparse loading. If the entirety of the 20 μL aliquot were evenly dispersed on the 18 mm diameter coverslip surface, the corresponding coverage would be on average less than $\frac{1}{2}$ molecule per square micron. This is an idealized case, in reality, much of the solution flies off the substrate during spin coating, likely producing areas with far lower density of molecules. The spot size may be larger than the distance between neighboring molecules; however, by employing a bi-analyte SMSERS protocol, this is not an issue. The rarity and locality of extremely enhancing regions on a PPA should allow observation of signal from only one isotopologue, which is proof for SMSERS.²⁵ Figure 5b shows a spectrum obtained from a PPA spin coated with both isotopogues demonstrating SERS of *only* R6G- d_0 superimposed on a fluorescent background. Arrows mark R6G- d_4 vibrational band locations at 610, 650, and 1342 relative cm^{-1} which are not present. Residual fluorescence is most likely due to R6G molecules adsorbed to the glass between the PPA's nanostructures. The observation of distinct SERS peaks above this fluorescence demonstrates the incredible level of signal enhancement produced by this periodic structure. Further experiments are underway to ensure statistical significance by collecting enough measurements which demonstrate a majority of signal from one or the other isotopologue. However, the spectrum in Figure 3b is an indication that NSL-derived plasmonic surfaces can indeed provide ample enhancement to enable single-molecule detection.

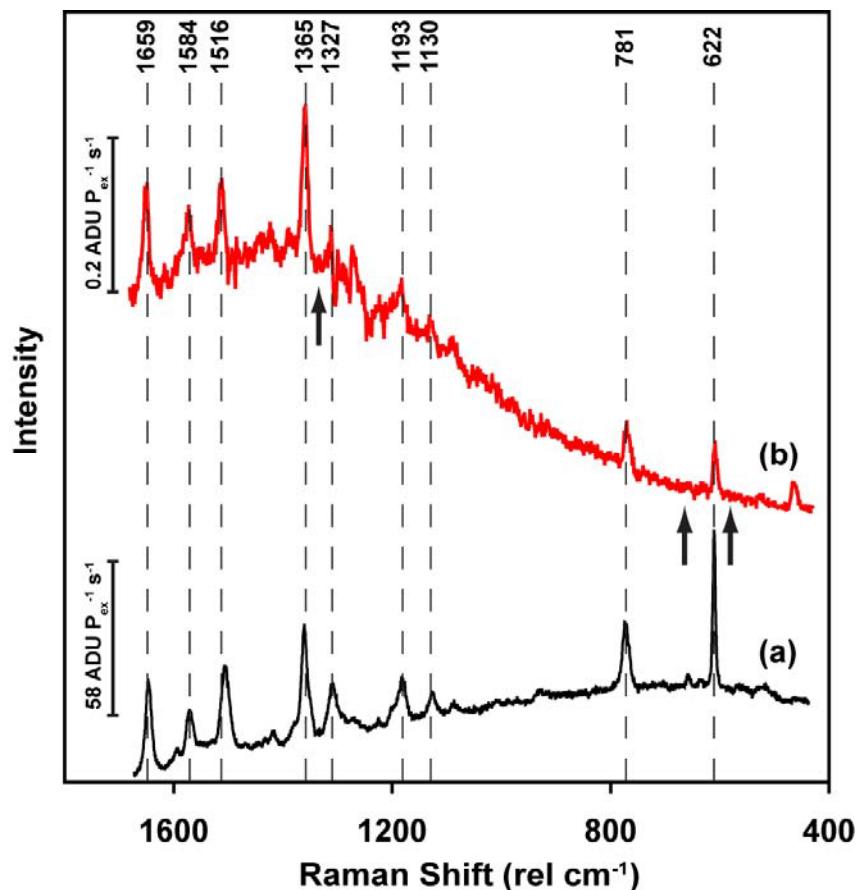


Figure 5. SERS spectra of R6G- d_0 : (a) on AgIF, (b) on PPA, with both isotopologues present.

5. CONCLUSIONS

Recent work in the Van Duyne group has focused on plasmonic nanostructures which demonstrate useful optical properties. The experiments outlined in this encompass fundamental to applied research topics and their intimate intersection. A wide-field LSPR imaging instrument was used to determine the refractive index sensitivity of multiple immobilized particles in parallel, significantly reducing experimental effort and increasing productivity. This versatile method was also used for parallel structure-function analysis and monitoring diffusion in media which mimic the viscosity of biologically interesting samples. Analysis of individual SERS nanotags provides fundamental insight into structural motifs which provide the greatest enhancement. Studying SMSERS of R6G on a PPA is a preliminary indicator that these scalable and easy to fabricate SERS substrates provide single molecule sensitivity. Many trials combine measurements of plasmonic properties with specific structural analysis, revealing relationships that are otherwise hidden by an ensemble averaged experiment or never measured. These fundamental and applied studies will continue to elucidate unanticipated structure-function relationships in plasmonic nanostructures and provide guidance for the optimization of plasmonic sensing platforms.

ACKNOWLEDGEMENTS

We thank Robert B. Lettan II and Prof. Karl Scheidt at Northwestern University for generously providing the deuterated rhodamine 6G isotopologue. This research was supported by the NSF (CHE-0911145), NSF NSEC (EEC-0118025), AFOSR/DARPA Project BAA07-61 (FA9550-08-1-0221), and the NSF MRSEC (DMR-0520513) at the Materials Research Center of Northwestern University. We thank the NUANCE center at Northwestern University for providing access to the TEM equipment.

REFERENCES

- [1] D. J. Barber, and I. C. Freestone, "An Investigation of the Origin of the Colour of the Lycurgus Cup by Analytical Transmission Electron Microscopy," *Archaeometry*, 32, 33-45 (1990).
- [2] K. A. Willets, and R. P. Van Duyne, "Localized Surface Plasmon Resonance Spectroscopy and Sensing," *Annual Review of Physical Chemistry*, 58, 267-297 (2007).
- [3] M. Faraday, "The Bakerian Lecture: Experimental Relations of Gold (and Other Metals) to Light," *Philosophical Transactions of the Royal Society of London*, 147, 145-181 (1857).
- [4] K. L. Kelly, E. Coronado, L. L. Zhao *et al.*, "The Optical Properties of Metal Nanoparticles: The Influence of Size, Shape, and Dielectric Environment," *Journal of Physical Chemistry B*, 107, 668-677 (2003).
- [5] P. L. Stiles, J. A. Dieringer, N. C. Shah *et al.*, "Surface-Enhanced Raman Spectroscopy," *Annual Review of Analytical Chemistry*, 1, 601-626 (2008).
- [6] W. E. Moerner, and D. P. Fromm, "Methods of single-molecule fluorescence spectroscopy and microscopy," *Review of Scientific Instruments*, 74(8), 3597-3619 (2003).
- [7] R. S. Krishnan, and R. K. Shankar, "Raman Effect: History of the Discovery," *Journal of Raman Spectroscopy*, 10(1), 1-8 (1981).
- [8] R. L. McCreery, [Raman Spectroscopy for Chemical Analysis] John Wiley & Sons, New York(2000).
- [9] D. L. Jeanmaire, and R. P. Van Duyne, "Surface Raman spectroelectrochemistry: Part I. Heterocyclic, aromatic, and aliphatic amines adsorbed on the anodized silver electrode," *Journal of Electroanalytical Chemistry*, 84(1), 1-20 (1977).
- [10] P. F. Liao, J. G. Bergman, D. S. Chemla *et al.*, "Surface-enhanced Raman scattering from microlithographic silver particle surfaces," *Chem. Phys. Lett*, 82, 355-359 (1981).
- [11] M. Kahl, E. Voges, S. Kostrewa *et al.*, "Periodically Structured Metallic Substrates for SERS," *Sensors and Actuators B: Chemical*, 51(1), 285-291(7) (1998).
- [12] J. C. Hulteen, and R. P. Van Duyne, "Nanosphere Lithography: A materials general fabrication process for PPA surfaces," *Journal of Vacuum Science Technology A*, 13(3), 1153-1558 (1995).
- [13] S. Nie, and S. R. Emory, "Probing Single Molecules and Single Nanoparticles by Surface-Enhanced Raman Scattering," *Science*, 275(5303), 1102-1106 (1997).

- [14] K. Kneipp, Y. Wang, H. Kneipp *et al.*, "Single Molecule Detection Using Surface-Enhanced Raman Scattering (SERS)," *Physical Review Letters*, 78(9), 1667-1670 (1997).
- [15] E. C. Le Ru, M. Meyer, and P. G. Etchegoin, "Proof of single-molecule sensitivity in SERS by means of a two-analyte technique," *Journal of Physical Chemistry B*, 110, 1944-1948 (2006).
- [16] J. A. Dieringer, R. B. Lettan, K. A. Scheidt *et al.*, "A frequency domain existence proof of single-molecule surface-enhanced Raman Spectroscopy," *Journal of the American Chemical Society*, 129(51), 16249-16256 (2007).
- [17] Y. Yamaguchi, H. Ishikawa, Y. Maruyama *et al.*, "Trigonal silver nanostructure for single molecule detection with surface enhanced raman scattering," *Journal of the Korean Physical Society*, 47, 856-862 (2005).
- [18] R. Jin, Y. Cao, C. A. Mirkin *et al.*, "Photoinduced Conversion of Silver Nanospheres to Nanoprisms," *Science*, 294, 1901-1903 (2001).
- [19] J. M. Bingham, K. A. Willets, N. C. Shah *et al.*, "Localized Surface Plasmon Resonance Imaging: Simultaneous Single Nanoparticle Spectroscopy and Diffusional Dynamics," *Journal of Physical Chemistry C*, 113, 16839-16842 (2009).
- [20] K. L. Wustholz, A. I. Henry, J. M. Bingham *et al.*, "Exploring single-molecule SERS and single-nanoparticle plasmon microscopy," *Proceedings of SPIE*, 7394, 739403-1-739403-10 (2009).
- [21] A. D. McFarland, and R. P. Van Duyne, "Single Silver Nanoparticles as Real-Time Optical Sensors with Zeptomole Sensitivity," *Nano Letters*, 3(8), 1057-1062 (2003).
- [22] L. J. Sherry, S.-H. Chang, B. J. Wiley *et al.*, "Localized Surface Plasmon Resonance Spectroscopy of Single Silver Nanocubes," *Nano Letters*, 5, 2034-2038 (2005).
- [23] L. J. Sherry, R. Jin, C. A. Mirkin *et al.*, "Localized Surface Plasmon Resonance Spectroscopy of Single Silver Triangular Nanoprisms," *Nano Letters*, 6(9), 2060-2065 (2006).
- [24] K. L. Wustholz, A. I. Henry, J. McMahon *et al.*, "Structure-Activity Relationships in Gold Nanoparticle Dimers and Trimers for Surface-Enhanced Raman Spectroscopy," *Journal of the American Chemical Society*, Accepted, (2010).
- [25] Y. Fang, N. Seong, and D. D. Dlott, "Measurement of the distribution of site enhancements in surface-enhanced raman scattering," *Science*, 321, 388-392 (2008).